
Article:
Krynkin, A. orcid.org/0000-0002-8495-691X, Dolcetti, G. and Hunting, S. (2017) Acoustic imaging in application to reconstruction of rough rigid surface with airborne ultrasound waves. Review of Scientific Instruments, 88. 024901 . ISSN 0034-6748

https://doi.org/10.1063/1.4974842

Acoustic imaging in application to reconstruction of rough rigid surface with airborne ultrasound waves

A. Krynkin,[1, a)] G. Dolcetti,[1] and S. Hunting[1]

Department of Mechanical Engineering, University of Sheffield, Mappin Street, Sheffield, S1 3JD, UK

(Dated: 12 January 2017)

[a)]a.krynkin@sheffield.ac.uk

ABSTRACT

Accurate reconstruction of the surface roughness is of high importance to various areas of science and engineering. One important application of this technology is for remote monitoring of open channel flows through observing its dynamic surface roughness. In this paper a novel airborne acoustic method of roughness reconstruction is proposed and tested with a static rigid rough surface. This method is based on the acoustic holography principle and Kirchhoff approximation which make use of acoustic pressure data collected at multiple receiver points spread along an arch. The Tikhonov regularisation and generalised cross validation (GCV) technique are used to solve the underdetermined system of equations for the acoustic pressures. The experimental data are collected above a roughness created with a 3D printer. For the given surface it is shown that the proposed method works well with the various number of receiver positions. In this paper, the tested ratios between the number of surface points at which the surface elevation can be reconstructed and number of receiver positions are 2.5, 5 and 7.5. It is shown that, in a region comparable with the projected size of the main directivity lobe, the method is able to reconstruct the spatial spectrum density of the actual surface elevation with the accuracy of 20%.

I. INTRODUCTION

It is highly attractive to be able to measure the hydraulic characteristics of an open channel flow from air. These types of flow are typical to rivers and partially filled pipes and it is of high importance to measure their hydraulic characteristics accurately and without submerging any instruments in them. One characteristic feature of these flows is rough water free surface. Evidence suggest that the surface roughness pattern of an open channel flow relates closely to their hydraulic charac-

teristics, e.g. Reynolds number and mean flow depth[1–3]. Therefore, measuring the parameters of this pattern, e.g. its spatial spectrum or correlation function, enables us to characterise the flow hydraulics and infer information about other processes which may develop in the flow for these set of the hydraulic conditions. As a first step towards the development of a technique that enables recovering these parameters, water surface can be considered frozen over a short period of time[4]. This can be justified by the fact that speed of sound in air $c_0 = 340$ m/s is much faster than the maximum phase velocity $U = U_0 + c_p$ (composed of flow velocity U_0 and the phase velocity of gravity waves c_p) at which surface rough patterns of shallow water flow propagate.

Range of inversion techniques has been proposed to reconstruct rough surface profile. In case when wavelength λ is much bigger than the surface roughness height ζ ($\zeta/\lambda \ll 1$) small perturbation method and Fourier transform can be used to directly reconstruct the surface profiles[5]. For the surfaces satisfying Kirchhoff criteria[6] and for both source and receiver positioned in the Fraunhofer zone with respect to the illuminated surface, variety of optical techniques have been developed to reconstruct surface profiles[7].

Airborne sound waves suit well for the inversion of the surface roughness of an open channel flow. Unlike in the case of electro-magnetic waves, the air-water interface characterised by rough surface is an acoustically rigid boundary so that an exact mathematical formulation for airborne sound pressure can be applied. In this paper it is proposed to use acoustic imaging techniques[8] which we develop further to recover the one-dimensional elevation of a static rough surface.

The acoustic imaging have been widely used to reconstruct the distribution of the acoustic sources on a known surface[9]. The original technique is built on the principles of the Near-field Acoustic Holography (NAH)[10] that requires single measurement due to the use of microphone array. Kirchhoff integral and convolution are at the

foundation of the NAH that makes method not restricted to the approximation of radiated/scattered acoustic pattern in the Fraunhofer zone. This measurement method offers a high spatial resolution where the characteristic spatial separation on the surface can be smaller than the acoustic wavelength. However the spatial resolution on the surface is restricted by the separation between the receivers[10].

An alternative holography method is to discretise Kirchhoff integral and to convert the boundary integral equations for the array of receivers into a matrix-based form[11]. In this direct method the number of receivers in the array can be much smaller than the number of points required to reconstruct distribution of sources on the surface. This leads to ill-conditioned matrix with multiple inverse solutions. The matrix inverse is based on the singular value decomposition method (SVD) and variety of regularisation methods such as truncated SVD and Tikhonov regularisation technique in conjunction with the methods optimising the choice of regularisation parameter[9,12,13]. In this paper the direct method based on the Kirchhoff integral discretisation is employed to reconstruct the elevation profile of a static, rigid rough surface.

With the idea in mind that the potential application of this method is to reconstruct the dynamically rough water surface, it is proposed to choose the surface elevation profile to be defined by a linear wave model that is based on the Fourier expansions with random phase and surface spectrum in form of the power function. This type of model has been used to study scattering of airborne electromagnetic waves by the ocean waves[15]. The representation of the surface spectrum as a power function of the wavenumber has wide applications in oceanography[16], and in water wave turbulence[17] and turbulence-generated surface roughness[18].

The paper is organised in the following manner. In Section II the geometrical parameters of surface profile are introduced. In this section, the parameters have been used in the linear wave model to generate surface which is manufactured with the

help of 3D printing technology. The section also introduces measurement technique. The acoustic source used in the measurements has been characterised by the directivity pattern modelled with the far-field approximation of the radiated sound by piston in a rigid baffle[14]. The diameter of the piston and frequency of the radiated sound results in narrow source directivity pattern that makes possible to neglect direct acoustic wave-field[1]. The measurement technique is based on a single microphone sliding along the circular arch. Normalising the recorded acoustic pressure by the signal sent to source removes phase offset and synchronises measurements combining all microphone locations into one single array[11]. The post-processing method is outlined in Section III. In order to isolate unknown surface profile the form of the Kirchhoff integral is simplified by introducing Kirchhoff approximation[1,6] and analysing scattered acoustic wave-field in the far-field with respect to the ratio between acoustic wavelength and surface-to-receiver/source distance. The acoustic wavelength is defined by acoustic source generating ultrasound at 43 kHz. It is proposed to discretise approximated Kirchhoff integral and apply SVD to obtain inverse solution. The surface profile is identified from the phase of the inverted integral. Section IV discusses application of the proposed post-processing technique to the collected data. The accuracy of reconstruction is compared for several sets of the measurements containing 60, 30 and 20 microphone locations.

II. ACOUSTIC MEASUREMENTS: GEOMETRY AND EXPERIMENTAL METHOD

A. Geometry of surface profile

In this work, the two-dimensional rough surface profile in Oxz Cartesian system of coordinates is generated through

$$\zeta(x) = \sigma \sum_n A_n \cos\left(K_n x + \tau_n\right), \tag{1}$$

where σ is the standard deviation of the rough surface, $K_n = 2\pi/l_n$ is wavenumber in the surface roughness spatial spectrum, τ_n is randomly generated phase. The amplitude A_n in the above equation is proportional to the wavelength l_n of the n-th harmonic in the Fourier expansion[15] so that

$$A_n \sim \left(\frac{2\pi}{l_n}\right)^{\alpha/2}. \tag{2}$$

and defined by the power spectrum slope α. Here it is chosen to use the spectrum with $\alpha = -2$ as a compromise between the resolution of the 3D printing technology and the requirements of the Kirchhoff approximation given by

$$\sin\psi > \frac{1}{(kh)^{1/3}}, \tag{3}$$

where h is a local curvature radius, k is the acoustic wavenumber and ψ is angle of an incident acoustic wave. The resulting spectrum is representative of a surface without strong harmonic components, which is typical of turbulent flows with small Froude number in the regimes from flat to wavy as identified by Brocchini and Peregrine[19]. For the rough surface analysed in this paper, the spatial scales were varied from $0.025 \leq l_n \leq 0.115$ m, and the standard deviation of the surface was set to $\sigma = 0.001m$. These values are consistent with the measurements of the free

n	A_n	K_n	τ_n
1	1.2	$\frac{2\pi}{0.115}$	-0.46
2	0.81	$\frac{2\pi}{0.0767}$	-0.08
3	0.49	$\frac{2\pi}{0.046}$	-0.83
4	0.35	$\frac{2\pi}{0.0329}$	-0.89
5	0.27	$\frac{2\pi}{0.0256}$	-0.76

TABLE I. Surface parameters used in the expansion (1)

surface of shallow turbulent flows[20]. The surface that was generated with equation (1) and used throughout this paper contains five terms ($n = 1..5$) in the expansion defined by the parameters in Table I

Figure 1(a) shows the elevation profile of this surface which is described by equation (1) with parameters defined in Table I. This surface profile was exported into commercial CAD software Solidworks 2014 where the drawing was converted into the format suitable for 3D printing technology. The results were loaded to the 3D printer Makerbot Replicator 2 which uses fused deposition modelling to print 3D objects. The printing material was Polylactic Acid with density $1250\,\mathrm{kg/m^3}$. For the selected 3D printing technique the printing accuracy is related to the minimum thickness of horizontal layers which is 0.0002 m. This is comparable with the standard deviation of the generated surface. In order to minimize printing error and to produce a smoother surface finish the printing process was carried out in vertical direction with surface built on the smallest side (thickness). Four separate tiles were produced and glued together to form a 0.46×0.3 m rough surface patch as shown in Figure 1(b). The length and width of each of these four tiles was set to 0.23 m and 0.15 m, respectively. Figure 1(b) shows the horizontal marks visible on the purple

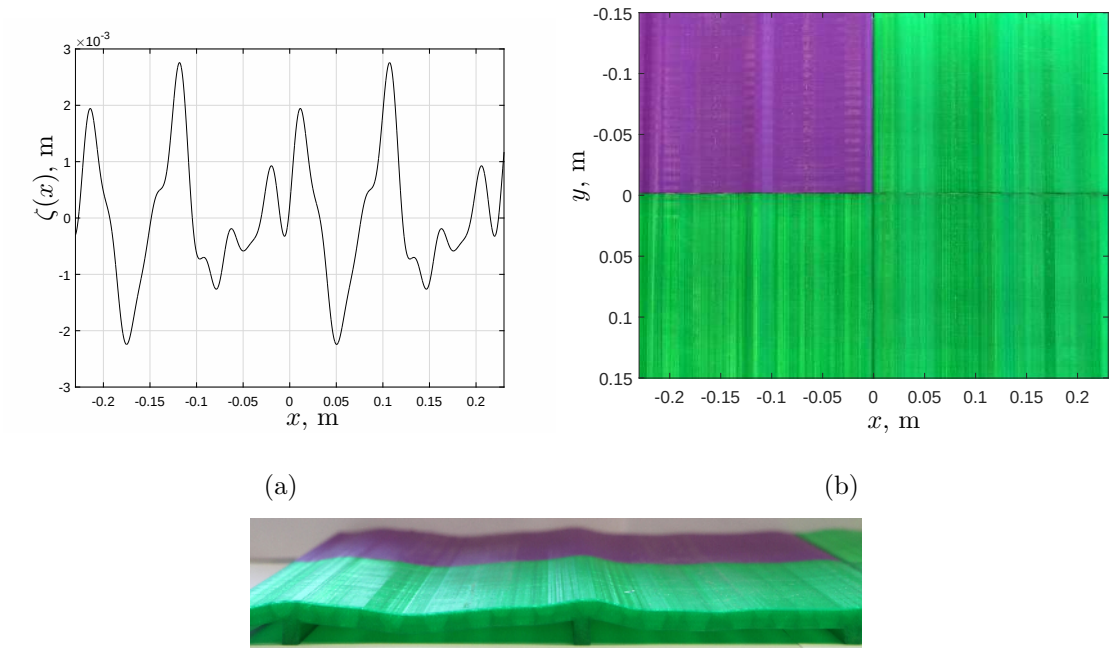

FIG. 1. Rough surface patch used in the reconstruction technique. (a) Surface profile. (b) Top view. (c) Side view of a single tile

tile (top left corner) which are left on the surface as a result of the vertical printing process. Three struts were printed on the underside of each of the four rough tiles to provide rigidity and to support profile when it is placed on a flat surface as illustrated in Figure 1(c). The set of the wavenumbers we adopted in equation (1) made the surface periodic with the period of 0.23 m. This periodicity ensured the continuity of the slope at the boundary between any two neighboring tiles. Along each of the four tiles the roughness profile was uniform along the y-direction (out of Oxz plane) in order to simulate the two-dimensional surface roughness.

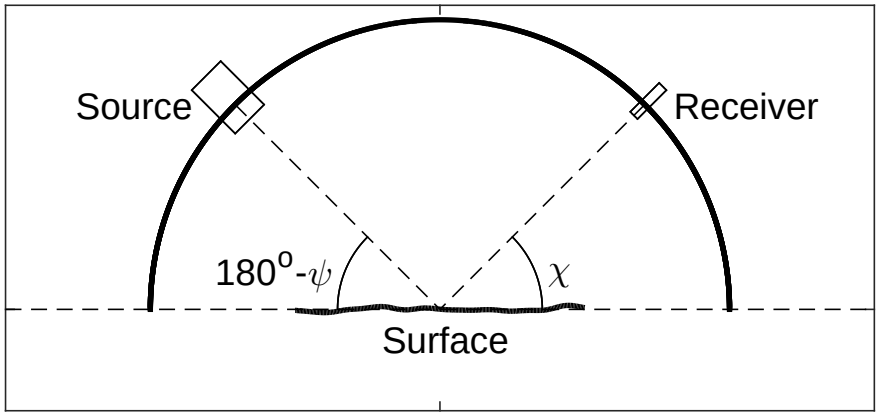

FIG. 2. Acoustic test rig

B. Acoustic equipment

For this work, the test rig was designed to support the source and receiver which were suspended over an arch above the rough surface patch as shown in Figure 2. The base of the rig was resting on the floor covered with absorbing material to reduce reflections at the side of the surface patch. The semi-circular shape of the rig was selected in order to record the forward scattered acoustic pressure field at multiple positions in along a semi-circle in Oxz plane. The radius of this arch was 0.4 m.

The source of sound was a $2a = 70$ mm diameter ultrasonic transducer (Pro-Wave ceramic type 043SR750) which was attached to one side of the arch insonifying the rough surface patch at $180^o - \psi$, where $\psi = 135^o$ measured from the Ox axis in counter-clockwise direction. A 1/4-in G.R.A.S. 46BF microphone, was attached to the opposite side of the arch. It was initially placed at angle 15^o to the surface and then moved towards 74^o at a 1^o angular increment. It enabled us to measure the acoustic pressure at 60 receiver positions along the arch within the $\chi = [15^o, 74^o]$ sector, where χ is the angle measured from the Ox axis at the centre of the arch in counter-clockwise direction. It is noted that both the microphone and ultrasonic

transducer protruded beyond the circumference of the arch towards the surface by 0.027 m and 0.017 m, respectively.

The ultrasonic transducer was driven at the frequency of $f = 43$ kHz with a 10 V peak to peak sinusoidal signal generated by a Tektronix AFG 3022C function generator. The far field directivity pattern of the source can be defined by the equation for an oscillating piston in a rigid baffle[14], i.e.

$$A(\phi) = \frac{J_1(ka\sin\phi)}{ka\sin\phi}, \tag{4}$$

where $k = 2\pi f/c_0$ is the acoustic wavenumber in air and

$$\phi = \arccos\left(\frac{z_s}{R_s}\right) - \left(\psi - \frac{\pi}{2}\right), \tag{5}$$

where the angle of incidence calculated in radians. In the above equation z_s is the z-coordinate of the source and $R_s = \sqrt{(x - x_s)^2 + z_s^2}$ is distance from the source to the point of observation at the mean surface $z = 0$[1].

The validity of the selected far-field source directivity pattern was experimentally validated and the results are illustrated in Figure 3. The measurement of the directivity pattern was conducted at 0.2 m and 1 m away from the transducer over 180^o angle sector. In order to isolate measured directivity pattern and compare it with equation (4) the collected magnitude of the radiated acoustic pressure was normalised by its maximum value found on the symmetry axis of the main lobe. Angle ϕ in these measurements was counted from the symmetry axis of the main lobe. It was found that the effective diameter of the transducer is 0.04 m compared to the actual diameter 0.07 m quoted by the manufacturer. The reduced value of the diameter gives the width of the main lobe which compares well with the measured directivity pattern with the accuracy within 1% of the measured results in angle sector containing the main lobe $[-10^o, 10^o]$.

It is noted that the directivity of the transducer and the length of the rough surface patch were chosen so that the main lobe in the directivity pattern fits the

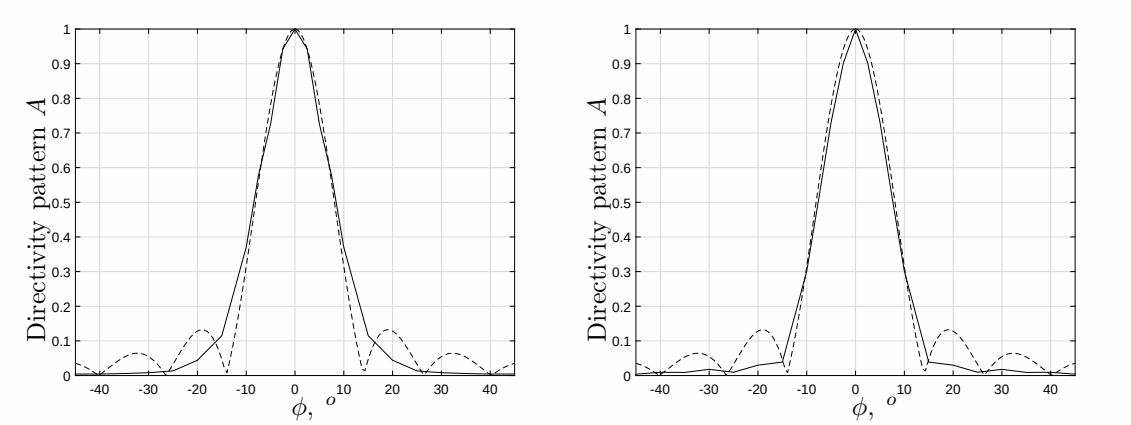

(a) (b)

FIG. 3. The measured (solid line) and predicted (dashed line) directivities of the sound source. Directivity patterns are plotted against angle ϕ from equation (4). Source-receiver distance is (a) 0.2 m and (b) 1m

size of the patch at distance 0.4 m when radiated at the angle of 135^o with the size of the project main lobe estimated at 0.2 m.

The experiments were carried out in the semi-anechoic chamber in order to reduce any possible secondary reflections and low-frequency structural vibration that could have altered the distance between the rough surface patch and receiver position. The equipment was assembled as shown in Figure 4. The signal generator was directly connected to the ultrasonic transducer. The microphone unit was connected to the G.R.A.S. power module type 12AK. Throughout all experiments its module settings 'Filter' and 'Gain' were fixed. The Filter dial was set to Lin which meant that there was no filtering of the data as their passed through the module. The Gain dial was set to +50 which amplified the power of the signal by 50 decibels. The G.R.A.S. power module and function generator (for reference signal) were connected to a 8 channels NI PXIe-6356 data acquisition (DAQ) card. The DAQ card was transferring

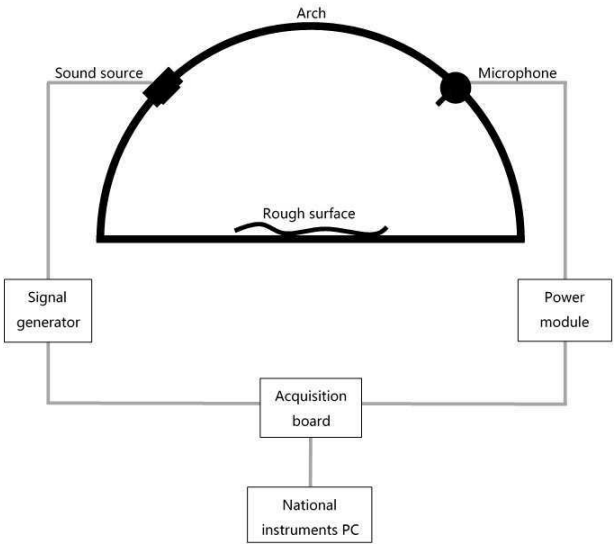

FIG. 4. Experimental setup diagram

data to a National Instruments (NI) PXIe-8108 embedded controller where a National Instruments LabView virtual instrument program was installed to record the acoustic signal at the 0.5 MHz sampling rate. At each position of the microphone reading was taken with a duration of 1 s. The microphone data and reference signal obtained directly from the signal generator were recorded synchronously. The resulting raw data were saved into text files so that analysis could be performed using commercial software Matlab R2015.

C. Experimental methodology

The recorded signal on microphone was first filtered with second order bandpass Butterworth filter defined in the 30 - 50 kHz frequency range. The Hilbert transform was applied to the acquired data to determine the signal amplitude $\mathcal{A}_{\Updownarrow}$ and phase τ_m at each of the 60 receiver positions. The transformed signal was then presented

in the following analytic form

$$P_m = \mathcal{A}_{\Updownarrow} \mathrm{e}^{i(2\pi f t + \tau_m)},\ m = 1..60. \tag{6}$$

These signals were then normalised against the reference signal obtained directly from the functional generator so that the complex acoustic pressure $\tilde{P}_m$ scattered by the rough surface to the given receiver point m along the arch can be written as

$$\tilde{P}_m = \tilde{\mathcal{A}}_m \mathrm{e}^{i\tau_m},\ m = 1..60, \tag{7}$$

where $\tilde{\mathcal{A}}_m$ is the normalised amplitude of the scattered acoustic signal at m-th receiver position. It is noted that normalised value is assumed to be independent on temporal variable that enables us to combine all the 60 microphone recordings to form a virtual array of receivers effectively yielding the directivity pattern recorded along the arch opposite to the sound source.

An example of the normalised amplitude and phase of the analytic signal recorded on the receiver at 15^o is shown in Figure 5. These data are plotted as a function of time and indicate that the both amplitude and phase varies with time. It is noted that amplitude varies within 25% from its mean value whereas phase varies within 10% from its mean value. This variation is associated with the characteristics of the ultrasonic transducer used in this experiment. In order to reconstruct the rough surface in this paper we selected the 1 sec average amplitude and phase values recorded at each of the 60 receiver positions.

III. KIRCHHOFF APPROXIMATION AND PSEUDO-INVERSE TECHNIQUE

In order to recover the rough surface profile we used the Kirchhoff approximation[21] which takes into account single reflection from the plane tangential to the surface.

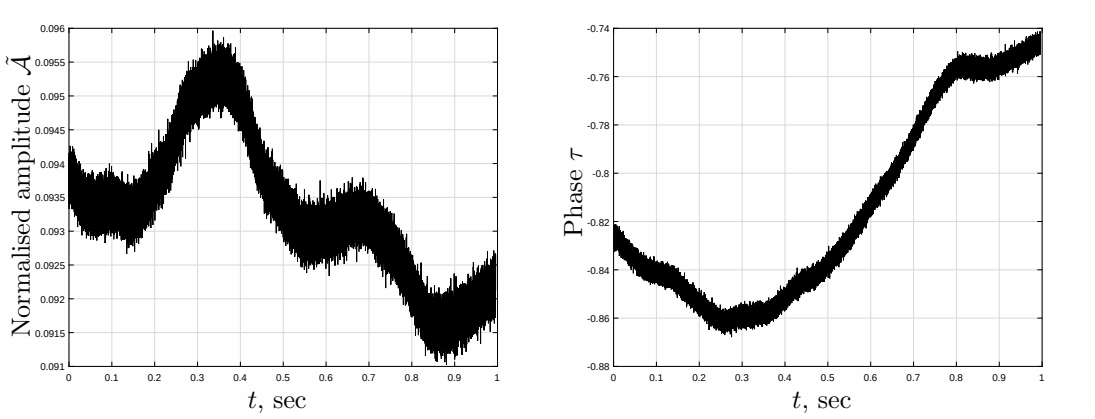

(a) (b)

FIG. 5. Amplitude (a) and phase (a) of the transformed signal recorded at 15^o to the surface

This limits the application of the proposed method to the surface that satisfy condition (3). Using this condition and assuming that source and receiver are in the far field from the reflecting surface ($kR \gg 1$ with R being characteristic distance to the surface) the acoustic pressure in 3D space can be approximated by the double integral over the mean plane S_0 (eq. (16) in Krynkin et al.[1]). Assuming that surface is uniform along the lateral coordinate axis Oy and that the surface dimension along Oy axis is much larger than the acoustic wavelength[21], the problem can be formulated in 2D space with the help of single integral written as

$$p(x_r, z_r) = -\frac{\mathrm{i}}{2\pi k} \int_{-\infty}^{+\infty} \frac{A(x)}{\sqrt{R_s R_r}} \exp\left[\mathrm{i}k(R_s + R_r) - \mathrm{i}q_z\zeta(x)\right] q_z \mathrm{d}x, \tag{8}$$

where $A(x)$ is directivity pattern given by equation (4), $\zeta(x)$ is surface elevation that needs to be reconstructed. The wavenumber q_z is given by

$$q_z = k\left(\frac{z_s}{R_s} + \frac{z_r}{R_r}\right). \tag{9}$$

Here $R_s = \sqrt{(x - x_s)^2 + z_s^2}$ and $R_r = \sqrt{(x - x_r)^2 + z_r^2}$ are the distances from the source and receiver to the specular reflection point at the mean surface $z = 0$[1], respectively. In this model the centre of Oxz plane is aligned with the centre of the semicircular arch as discussed in Section II B so that the coordinates of the source (x_s, z_s) and receiver (x_r, z_r) can be expressed in the form of polar coordinates with radial distance fixed at the radius R of the arch. This gives

$$\begin{aligned}(x_s, z_s) &= R(\cos\psi, \sin\psi) \\ (x_r, z_r) &= R(\cos\chi, \sin\chi).\end{aligned} \tag{10}$$

In the presence of surface roughness scales comparable with the acoustic wavelength, the number of required surface points for adequate reconstruction M inevitably becomes greater than the number of the available receivers N. In practical applications, the maximum number of receivers N is restricted by technical limitations and by the amount of data which can be processed. Arranging the discretised integral (8) over the surface S_0 with the M uniform spatial elements $\Delta x = x_{m+1} - x_m$, $m = 1, ..., M-1$ for all N receivers into a matrix form results in the under-determined system which can be inverted with the help of singular value decomposition technique (SVD)[8]. This gives

$$\boldsymbol{P}_{N\times 1} = \boldsymbol{H}_{N\times M}\boldsymbol{E}_{M\times 1}, \tag{11}$$

where $\boldsymbol{P}_{N\times 1}$ is a vector containing recorded acoustic signal at the N receiver locations. The elements of the matrix $\boldsymbol{H}_{N\times M}$ and vector $\boldsymbol{E}_{M\times 1}$ are given by

$$h_{mn} = \left\{ -\frac{\mathrm{i}}{2\pi k}\frac{A(x_{mn})}{\sqrt{R_{s,mn}R_{r,mn}}}\exp\left[\mathrm{i}k(R_{s,mn} + R_{r,mn})\right] q_{z,mn}\Delta x \right\}_{m=1,...,M, n=1,...,N} \tag{12}$$

$$e_m = \left\{\exp\left[-\mathrm{i}q^s_{z,m}\zeta(x_m)\right]\right\}_{m=1,...,M}, \tag{13}$$

respectively. We note that the elements of the vector $\boldsymbol{E}_{M\times 1}$ are defined by the receiver aligned with the specular reflection point for the source being at $\psi = 135^o$, i.e. with $\chi = 45^o$. We also assume that q_z in equation (8) is approximately constant for all the receivers with the value given by the direction specular to that of the source, $q_z^s(x_m) = 2kz_s/R_s$.

The resulting ill-conditioned matrix can be regularised with the help of Tikhonov regularization technique[13] and the surface elevation at point x_m can be approximated with

$$\{\zeta_m\}_{m=1,\ldots,M} = \left\{ \frac{\mathrm{iLn}(e_m)}{q^s_{z,m}} \right\}_{m=1,\ldots,M}, \tag{14}$$

where e_m is defined by equation (13). The application of the SVD[22] to equation (11) gives

$$\boldsymbol{E}_{M\times 1} = \mathrm{svd}^{-1}(\boldsymbol{H}_{N\times M})\boldsymbol{P}_{N\times 1}, \tag{15}$$

where operator svd^{-1} defines inversion of the matrix $\boldsymbol{H}_{N\times M}$ decomposed into the product of unitary matrices $\boldsymbol{U}_{N\times N}$ and $\boldsymbol{V}_{M\times M}$ and a diagonal matrix $\boldsymbol{S}_{N\times M}$ with nonnegative elements arranged in the descending order of smallness that is

$$\mathrm{svd}(\boldsymbol{H}_{N\times M}) = \boldsymbol{U}_{N\times N}\boldsymbol{S}_{N\times M}\bar{\boldsymbol{V}}^T_{M\times M}, \tag{16}$$

where $\bar{\mathbf{A}}$ stands for complex conjugate and $\mathbf{A}^T$ denotes matrix transpose. Equation (15) is conditioned with the Tikhonov regularisation parameter β identified with the help of generalised cross validation (GCV) technique[13]. The application of the SVD in equation (15) is performed with a library function available in commercial software Matlab R2015a.

IV. SURFACE RECONSTRUCTION RESULTS

The results of the application of the proposed reconstruction technique (equation (14)) to the measured acoustic pressures $\boldsymbol{P}$ at $N = 60$, 30 and 20 positions is il-

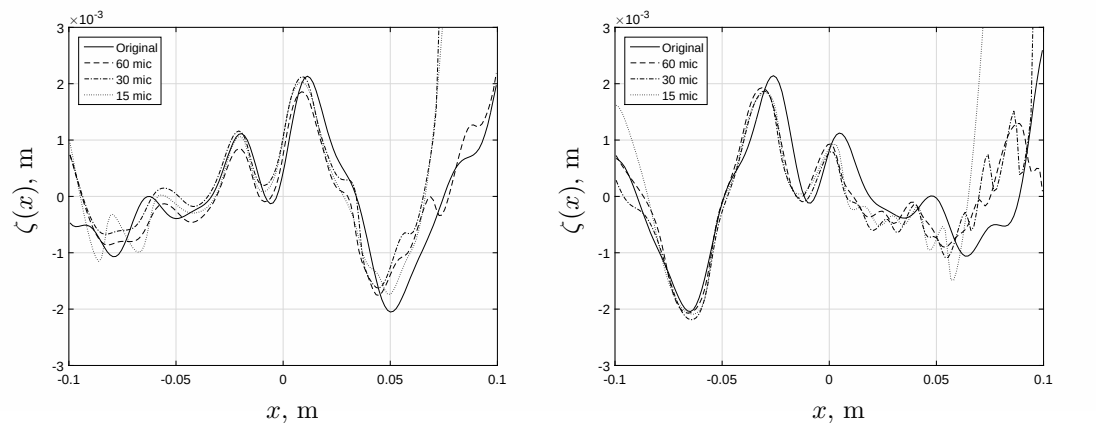

FIG. 6. The reconstructed surface roughness (dashed, dash-dot and dotted lines) and the actual surface roughness (solid line). (a) Receiver orientation A; (b) receiver orientation B.

lustrated in Figure 6. For the reduced number of receivers ($N = 30$ and $N = 20$) the separation between the receivers was increased to 2^o and 3^o, respectively. Due to the directivity of the source and fixed value of the q_z^s at specular point $\chi = 45^o$ in the definition of vector $\boldsymbol{E}_{M\times 1}$ in equation (13), the proposed inversion technique does not allow the reconstruction of the surface roughness outside of the illuminated patch which length was approximately 0.2 m. Therefore, all the presented results are restricted to the spatial interval $-0.1 \leq x \leq 0.1$ m. The total number of points recovered within this interval is 150 (that is $M = 150$) that scales in the ~ 1 mm spatial resolution.

The reconstruction technique was applied to the acoustic pressures, $\boldsymbol{P}_{N\times 1}$, measured when the rough surface was oriented in two particular ways. The first set of acoustic pressures was measured when the rough patch was installed in orientation A (purple colored tile in the top left corner as illustrated in Figure 1(b)) with

respect to the arch. The second set of acoustic pressures was measured when the rough patch was installed in orientation B (purple colored tile in the bottom right corner) with respect to the arch. Due to the asymmetric surface profile along the Ox axis with the central point in the middle of the rough surface patch the two data sets can be associated with acoustic scattering over two different surfaces. Figure 6 demonstrates that the proposed method is able to reconstruct a wide range of roughness scales with 10 % error in roughness standard deviation $\sigma = 1$ mm for 60 receivers (dashed line in Figure (6)). The roughness profile reconstructed for the both patch orientations is shifted along the Ox axis that can be explained by the non-uniform distribution of the receiver positions along the arch. The uncertainty in receiver positioning is estimated at ± 0.005 m that reduces the resolution of the reconstruction technique. In this experiment the resolution with which the surface can be reconstructed is ± 0.5 mm defined through the absolute root mean square error in the roughness wave height.

The inversion of the under-determined system can result in the appearance of ghost scales which are observed closer to the edge of the area of rough patch illuminated by the source. This can also reduce the accuracy of the reconstruction technique. In particular, the reconstructed surface contains smaller scales near $x = 0.1$ m which can be observed in Figures 6. This point is near the edge of the area of the patch illuminated by the directional source. It is also noted that the decrease in the number of receivers generally results in the decrease of the surface area which can be accurately reconstructed. This is observed in Figures 6(a) and (b) for 30 and 20 receivers with inadequate representation of the surface scales in the spatial interval $0.05 \leq x \leq 0.1$ m. In this interval the error in reconstructed roughness standard deviation increases from 10% for 60 receivers to 200% for 20 receivers. However in the shorter spatial interval, namely $-0.05 \leq x \leq 0.05$, the error in the reconstructed roughness standard deviation is below 2%. It must be noted that in the shorter

spatial interval the original standard deviation $\sigma = 1$ mm is reduced to 0.75 mm.

In many applications it is of importance to estimate the spatial spectrum of the roughness to understand the range of roughness scales and their relative amplitude[23]. In order to estimate how accurate the reconstruction is, it was proposed to compare the normalised power spectrum of the two roughness profiles reconstructed with the proposed inversion technique over the spatial interval of length $L = 0.2$. The spatial power spectrum was calculated as

$$F_\zeta(K) = \left(\left| \frac{1}{2\pi L} \int_{-L/2}^{L/2} \zeta(x) \mathrm{e}^{-\mathrm{i}Kx} \mathrm{d}x \right| \right)^2, \tag{17}$$

where K is the spatial wavenumber. Figures 7 presents the original and reconstructed power spectra of the two surface realisations plotted against the spatial wavenumber. These spectra were normalised against their maximum values. The results shown in Figures 7(a) and (b) suggest that the inversion technique is able to estimate accurately a broad range of the roughness scales for $K_1 \leq K \leq K_5$, where K_1 and K_5 indicate the cut-on and cut-off scales in the inversion. These are shown with the vertical solid lines in Figures 7(a) and (b). The accuracy of the proposed method was then estimated for $K_1 \leq K_n \leq K_5$, where $K_n = 2\pi/l_n$, $n = 1..5$, and the two spatial scales in equation 1 were $l_1 = 0.115$ m and $l_5 = 0.0256$ m (see Table I). The mean relative error was then calculated as

$$\epsilon = \frac{\sum_{n=1}^{N_K} \left[F_\zeta(K_n) - F_{\tilde{\zeta}}(K_n) \right]}{\sum_{n=1}^{N_K} F_\zeta(K_n)}, \tag{18}$$

where $N_K = 5$ is total number of the power spectrum points in $[K_1, K_5]$ interval, $F_{\tilde{\zeta}}(K_n)$ and $F_\zeta(K_n)$ are the power spectrum (17) of reconstructed surface profile and actual roughness, respectively. In the $K_1 \leq K \leq K_5$ interval the reconstruction error with 60 receivers is $\epsilon = 13\%$ in the case of orientation A. The reconstruction error with 60 receivers is 18% in the case of orientation B. The reconstruction error

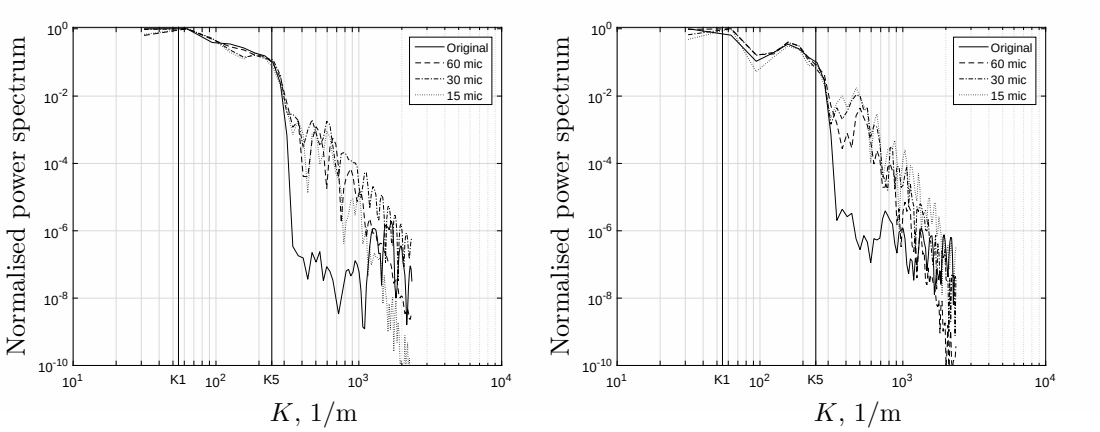

FIG. 7. The normalised power spectrum of the reconstructed surface (dashed, dash-dot and dotted lines) and spectra of the original surface (solid line). $K_1 = 54.6$ 1/m and $K_5 = 245.9$ 1/m. (a) Surface orientation A; (b) Surface orientation B.

improves for smaller surface scales as the number of receivers reduces. This can be explained by the presence of the 'ghost' scales. The above errors became 5% (orientation A) and 17% (orientation B) when the number of receivers was reduced to 30. For 20 receivers these errors were 3% and 8%, respectively.

It is also visible in Figures 7 that The reconstruction error increases for larger surface scales as the number of receivers reduces This can be explained by the decrease in the ability of the algorithm with fewer receivers to reconstruct the surface roughness along the whole length of the illuminated patch as it is illustrated in Figures 6.

V. CONCLUSION

In this paper the matrix based inverse technique has been applied to reconstruct a static rough surface profile. The proposed technique is based on the discretised Kirchhoff approximation integrals formulated at the multiple receiver positions over a flat surface. The resultant system of linear equations has been solved with the help of the singular value decomposition method.

The acoustic pressures measured with the single microphone sliding along the circular arch have been post-processed to remove the phase offset and to determine their amplitude and phase. With the aim to recover sub-centimetre roughness scales the required number of points on the surface is bigger than the number of available receivers. This has led to the under-determined problem that has been regularised with Tikhonov regularisation technique to stabilise the matrix solution. It has been shown that the proposed inversion technique can result in the 'ghost' scales observed at the edges of the reconstructed area of roughness. This can be explained by the fact that a point at which the surface roughness is reconstructed had to be in the proximity of an acoustic source specular point. This specular reflection point is defined by the main axis of the source directivity pattern.

The inverse technique discussed in this paper has been able to recover the surface roughness within the ± 0.1 m area illuminated by the adopted piezo-ceramic transducer. The reconstruction technique has been tested for 20, 30 and 60 synchronised receivers. The recovery of the spatial scales has been analysed with the power spectral density. In case of 60 receivers all scales present on the surface have been reconstructed with mean error of up to 18%. This error decreases with the reduction in the number of receivers to less than 10% for 20 receivers. The error decrease in the reconstructed power spectrum can be explained by the effect of 'ghost' scales.

Further improvements of the proposed technique may require the use of differ-

ent source/receivers combinations, simultaneous use of multiple receivers and less directional sources of sound.

ACKNOWLEDGEMENT

The authors wish to thank Professor Kirill V Horoshenkov for his valuable comments and suggestions for this manuscript. The authors would also like to thank the anonymous reviewers of this paper for constructive comments.

REFERENCES

[1]A. Krynkin, K. V. Horoshenkov, A. Nichols and S. J. Tait, Review of Scientific Instruments, 85, 114902 (2014)

[2]A. Nichols, S. J. Tait, K. V. Horoshenkov and S.J. Shepherd, Journal of Hydraulic Research, 0, 1 (2016)

[3]G. Dolcetti, K. V. Horoshenkov, A. Krynkin, and S. J. Tait, Physics of Fluids, 28, 105105 (2016)

[4]A. Nichols, S. J. Tait, K. V. Horoshenkov and S.J. Shepherd, Flow Measurement and Instrumentation, 34, 118–126 (2013)

[5]R.J. Wombell and J.A. DeSanto, "The reconstruction of shallow rough-surface profiles from scattered field data," Inverse Problems, 7, 7–12 (1991).

[6]E.I. Thorsos, J. Acoust. Soc. Am., 83, 78 (1988)

[7]C.J.R. Sheppard, Waves Random Media, 8, 53 (1998)

[8]A. Schuhmacher, J. Hald, K.B. Rasmussen and P.C. Hansen, J. Acoust. Soc. Am., 113, 114 (2003)

[9]N. Totaro, D. Vigoureux, Q. Leclére, J. Lagneaux, J.L. Guyader, Journal of Sound and Vibration, 336, 62 (2015)

[10]J.D. Maynard, E.G. Williams, and Y. Lee, J. Acoust. Soc. Am., 78, 1395 (1985)

[11]E.G. Williams and B.H. Houston, J. Acoust. Soc. Am., 114, 1322 (2003)

[12]P.A. Nelson and S.H. Yoon, Journal of Sound and Vibration, 233, 643 (2000)

[13]Q. Leclére, J. Sound Vib., 321, 605 (2009).

[14]P.M. Morse and K. Uno Ingard, *Theoretical acoustics* (McGraw-Hill, New York, 1968) p. 381.

[15]Toporkov and G.S. Brown, IEEE Trans. Geosc. Remote Sens., 38, 4 (2000)

[16]O. M. Phillips, Journal of Fluid Mechanics, 4, 426 (1958)

[17]V. E. Zakharov and N. N. Filonenko, Journal of applied mechanics and technical physics, 8, 37 (1967)

[18]V. Borue, S. A. Orszag, I. Staroselsky, Journal of Fluid Mechanics, 286, 1 (1995)

[19]M. Brocchini and D. H. Peregrine, Journal of Fluid Mechanics, 449, 225 (2001)

[20]K. V. Horoshenkov, A. Nichols, S. J. Tait, G. A. Maximov, Journal of Geophysical Research: Earth Surface, 118, 1864 (2013)

[21]F. G. Bass and I. M Fuks, *Wave Scattering from Statistically Rough Surfaces* (Pergamon, Oxford, 1979) p. 186.

[22]`http://uk.mathworks.com/help/matlab/ref/svd.html` (Assessed on 25.05.2016)

[23]A. Ishimaru, *Wave propagation and scattering in random media* (Academic Press, New York, 1978) p. 504.